Information Sciences 296 (2015) 14–24

Contents lists available at ScienceDirect

Information Sciences

journal homepage: www.elsevier.com/locate/ins

Exudate segmentation in fundus images using an ant colony optimization approach

Carla Pereira [a,*], Luís Gonçalves [b], Manuel Ferreira [a,c]

[a] Centro Algoritmi, University of Minho, Campus Azurém, 4800-058 Guimarães, Portugal
[b] Oftalmocenter, Azurém, 4800-045 Guimarães, Portugal
[c] ENERMETER, Parque Industrial Celeirós, Lugar de Gaião – Lotes 5/6, 4705-025 Braga, Portugal

ARTICLE INFO

Article history:
Received 3 January 2013
Received in revised form 20 October 2014
Accepted 27 October 2014
Available online 4 November 2014

Keywords:
Ant colony optimization
Exudate
Fundus image
Image processing
Multi-agent system

ABSTRACT

The leading cause of new blindness and vision defects in working-age people, diabetic retinopathy is a serious public health problem in developed countries. Automatic identification of diabetic retinopathy lesions, such as exudates, in fundus images can contribute to early diagnosis. Currently, many studies in the literature have reported on segmenting exudates, but none of the methods performs as needed. Moreover, several approaches were tested in independent databases, and the approach's capacity to generalize was not proved. The present study aims to segment exudates with a new unsupervised approach based on the ant colony optimization algorithm. The algorithm's performance was evaluated with a dataset available online, and the experimental results showed that this algorithm performs better than the traditional Kirsch filter in detecting exudates.

1. Introduction

Diabetic retinopathy (DR) is an eye disease associated with long-standing diabetes mellitus, which causes abnormalities in the retina. DR has become a serious public health problem in developed countries, since it is the leading cause of new blindness and vision defects in working-age individuals. In the initial stages of DR, patients are generally asymptomatic, but in the more advanced phase, they may experience symptoms that include distortion and blurred vision. Therefore, early detection of DR is crucial for preventing vision impairment and for effective treatment. The easiest method for analyzing the eye fundus in screening programs for preventing DR is digital color fundus photographs. They create a high-quality record of the fundus for detecting DR early signs and monitoring its progression. However, due to the growing incidence of diabetes in the population, ophthalmologists must examine a huge number of images. Therefore, developing computational tools that can assist diagnoses is of major importance.

Exudates are one of the earliest signs of DR. They indicate increased vessel permeability since they are plasma lipid and protein accumulations in the retina. In fundus images, exudates appear as shiny yellow–white dots with sharp borders. Exudates are frequently observed with microaneurysms, characteristic dark DR lesions. The problems in accurately detecting exudates in fundus images are noise presence, low contrast, uneven illumination, and color variation. Several approaches have been proposed in the literature to segment this type of lesion from color fundus photographs. Giancardo et al. [10] roughly divided the approaches into four categories: thresholding, morphology, region growing, and supervised methods.

* Corresponding author.
E-mail address: id2723@alunos.uminho.pt (C. Pereira).

http://dx.doi.org/10.1016/j.ins.2014.10.059
0020-0255/

Thresholding methods are based on global or local gray-level analysis. For instance, Sanchez et al. [24] presented a thresholding method based on a statistical mixture model. This method was used on the enhanced image histogram to determine a dynamic threshold for each image. Then, a postprocessing technique based on edge detection using Kirsch's method was applied to distinguish hard exudates from other bright lesions.

Morphology methods consist of applying morphological operators to identify structures with specific shapes (such as vessels). These structures are then removed, and exudates can be selected [3,23,25,28,29]. Morphological operators are sometimes combined with other techniques such as contrast enhancement and clustering methods [3].

Region growing methods segment the image based on spatial gray-level contiguity. For instance, Li and Chutatape [15] used CIE Luv color space images and applied a region growing method proceeded by the Canny edge detector. Edge detection decreases the size of the regions and significantly decreases the computation time.

Supervised methods are the most common in the literature [7,8,10,12,20,21]. They consist of building a feature vector for each pixel or pixel cluster, to be classified with a machine learning approach into exudates or non-exudates. The features are based on the color, brightness, size, shape, edge strength, texture, and contextual information of pixel clusters. The machine learning methods commonly used are neural networks [8,21], support vector machines (SVMs) [7,10], linear discriminant classifiers [12,20], the Naïve Bayes classifier [10], and the random forest algorithm [32]. A hybrid classifier as an ensemble of a Gaussian mixture model and an SVM was proposed in [1].

The problem with supervised approaches is that numerous manually labeled data are needed. Ali et al. [2] created a retinal atlas image with a set of healthy fundus images and then detected the bright lesions by determining the chromatic differences between the atlas images and an image of a diseased eye.

The results for these approaches are summarized in Table 1. Unfortunately, the majority of these algorithms were tested in independent databases with different characteristics. Therefore, it is not possible to prove the approaches' capacity to generalize. Moreover, the results were quantified using different evaluation methods, which makes comparing the results difficult.

Table 1
Results and methodology categories of approaches in the literature.

Author	Method category	Results	Dataset
Walter et al. (2002)	Morphology	Sensitivity/predictive value pair of 92.8%/92.4% (per lesion)	30 Images: 15 with exudates
Li et al. (2004)	Region growing	Sensitivity/specificity pair of 100%/71 % (per image)	35 Images with exudates
Fleming et al. (2007)	Supervised	Sensitivity/specificity pair of 95%/84.6% (per image)	13 219 Images: 300 with exudates
Niemeijer et al. (2007)	Supervised	Area under ROC curve = 0.95; sensitivity/specificity pair of 95%/88% for detecting bright lesions of any type (per lesion)	300 Images: 100 with bright lesions and 200 without
Sanchez et al. (2008)	Supervised	Sensitivity of 88% and mean number of false positive per image of 4.83 ± 4.64 (per lesion); sensitivity/specificity pair of 100%/100% (per image)	83 Images: 25 for training and 58 for testing (36 with exudates)
Sopharak et al. (2008)	Morphology	Sensitivity/specificity pair of 80%/99.5% (per lesion)	60 Images: 40 with exudates
García et al. (2009)	Supervised	Sensitivity/predictive value pairs of 88.1%/80.7 % with MLP, 88.5%/77.4 with RBF, 87.6%/83.5% with SVM (per lesion) and sensitivity/specificity pairs of 100%/92.5% with MLP, 100%/81.5% with RBF, 100%/77.8% with SVM (per image)	117 Images: 50 for training and 67 for testing (40 with DR signs)
Ravishankar et al. (2009)	Morphology	Sensitivity/specificity pairs of 94.6%/ 91.1% (per pixel) and 95.7%/94.2% (per image)	516 Images: 345 with exudates
Sanchez et al. (2009)	Dynamic thresholding	Sensitivity/predictive value pair of 90.2%/96.8% (per lesion) and sensitivity/specificity pair of 100%/90% (per image)	106 Images: 26 for training and 80 for testing (40 images with exudates)
Osareh (2009)	Supervised	Sensitivity/specificity pair of 96%/94.6% (per image) and sensitivity/predictive value pair of 93.5%/92.1% (pixel level)	300 Images: 150 with DR signs
Welfer (2009)	Morphology	Sensitivity/specificity pair of 70.5%/98.8 % (per image)	DIARETDB1
Amel (2012)	Morphology	Sensitivity/predictive value pair of 95.9%/92.3%	50 Images from MESSIDOR
Giancardo (2012)	Supervised	Area under ROC curve between 0.88 and 0.94 depending on the dataset/features used	MESSIDOR; HEI-MED and DIARETDB1
Ali (2013)	–	Accuracy of 82.60% (per lesion)	HEI-MED
Akram (2014)	Supervised	97.3%, 95.9% and 96.8% for sensitivity, specificity and accuracy, respectively (per lesion)	MESSIDOR and HEI-MED
Zhang (2014)	Supervised	Area under ROC curve between 0.93 and 0.95 depending on the dataset/features used	MESSIDOR; HEI-MED and DIARETDB1

In this study, a new approach for segmenting exudates is proposed based on ant colony optimization (ACO). ACO is a branch of a larger field referred to as swarm intelligence (SI) and is inspired by observation of the collective foraging behavior of real ant colonies. Using artificial ant colonies, the problem solutions are constructed within a stochastic iterative process by adding solution components to partial solutions. Each ant constructs a part of the solution using artificial pheromone, which reflects the ant's accumulated experience and heuristic information depending on the problem [6]. The ACO algorithm has been used in digital image processing with different purposes such as edge detection [27,31], image segmentation [13,17,26], visual saliency detection [16], and image thresholding [19]. ACO has been used in fundus images to locate the OD [14,22] and segment retinal blood vessels [4,11]. However, this type of approach has never been applied to retinal images to detect DR lesions.

The paper is organized as follows: In Section 2, the proposed approach is described. The results are shown and discussed in Section 3. Finally, the conclusion is presented in Section 4.

2. Methods

Since exudates have the highest contrast with the background in the green plane of the RGB color model [28], this model was chosen to implement the proposed approach. This approach is mainly constituted by two parts. First, a preprocessing phase was developed to find a binary image with exudate candidates based on its high-intensity gray level. Since the sharpness of the exudate edges is an important attribute that distinguishes them from other bright lesions [12], edge strength for each candidate was then evaluated. This was performed by analyzing the image that resulted when ACO was applied in 128×128 image windows. An outline of the proposed approach is illustrated in Fig. 1.

For evaluating the edge strength with different pre-processing phases, other authors [9,12,24] used a traditional edge detector, the Kirsch filter. In order to compare the new approach with those approaches, part of Giancardo et al.'s method [9] was also implemented and evaluated in the same way.

2.1. Preprocessing

The intra- and inter-image variability of fundus images, mainly due to retinal pigmentation and the acquisition process, affects automatic segmentation of exudates. Therefore, a preprocessing step for normalizing images is very important to improve the algorithm capacity for generalizing.

The variation in intensity in the background across the image can be eliminated by estimating the background image (I_b) and subtracting that from the original green plane image (I_{green}). The I_b is estimated by applying a median filter with a 50×50 pixel kernel. The size of this filter was chosen according to the widest blood vessel in the database. The shaded corrected image (I_{sc}) shows the characteristic gray-level distribution: The highest histogram peak is always centered on zero, and there is a clear distinction between dark and bright structures. The left histogram tail with negative values belongs to dark structures such as vessels, the macula, and dark lesions. The positive histogram tail corresponds to the bright structures including the optic disk, bright lesions, and other bright structures. Fig. 2 shows three color retinal images and the respective green plane image, normalized gray-level image, and normalized I_{sc} histogram (from left to right).

At this point and since all the normalized images have similar histogram characteristics, it is possible to select all the exudate candidates with a simple hard threshold. However, it was experimentally noticed that the use of two hard thresholds with posterior morphological reconstruction can improve results (Fig. 3). Applying a low threshold value (T_1) permits the selection of all exudates and respective borders. With a higher threshold value (T_2), the bright intensity peaks, which mostly correspond to exudates, are detected. In fact, in that way it is possible to eliminate several false positives and maintain the borders of the correct candidates that are really exudates. The values for T_1 and T_2, experimentally determined, were 0.008 and 0.02, respectively. In the binary image (I_{cand}), all bright lesions should be identified.

The preprocessing step finalizes with the candidates that belong to the optic disk (OD) being eliminated. The OD was detected with the method described in [22].

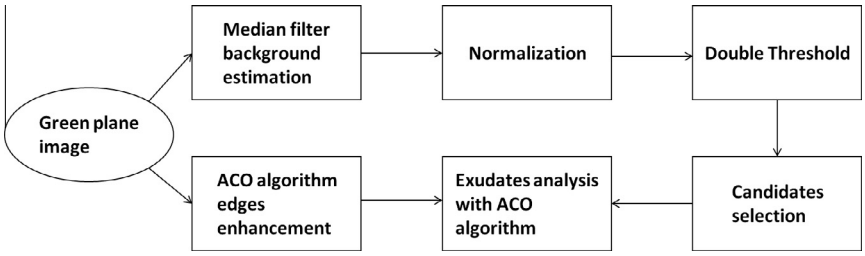

Fig. 1. Schematic representation of the proposed approach.

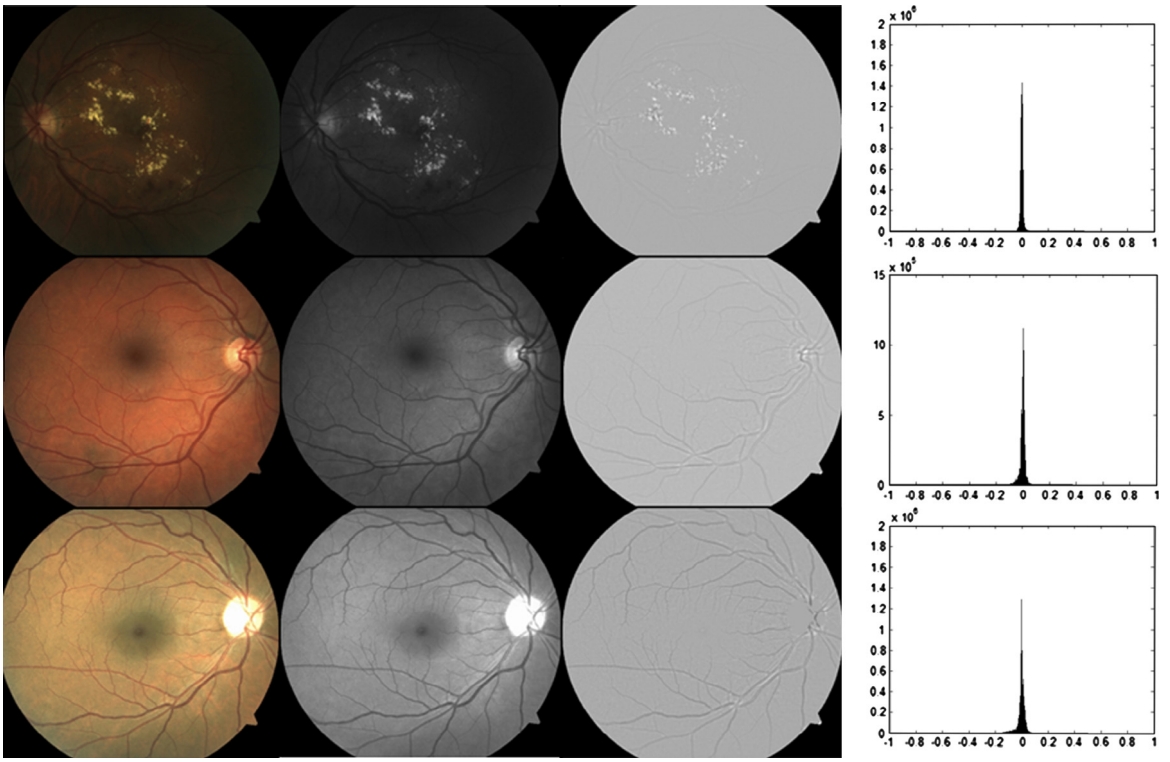

Fig. 2. From left to right: original color image; green plane image; normalized gray level image; normalized image histogram. (For interpretation of the references to color in this figure legend, the reader is referred to the web version of this article.)

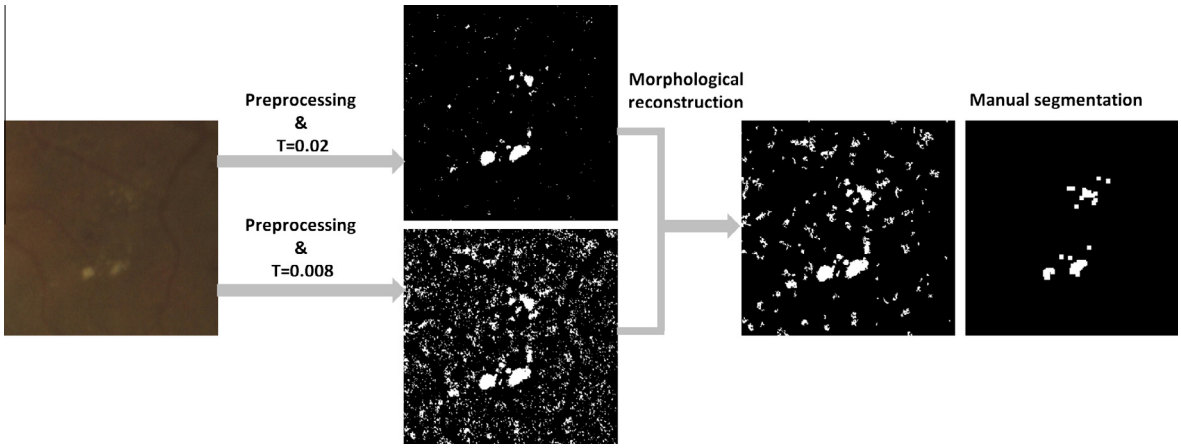

Fig. 3. Using two hard thresholds with posterior morphological reconstruction eliminates a number of false positives and maintains the correct candidates' border.

2.2. Ant colony optimization algorithm

The ACO algorithm was first introduced and formalized as a meta-heuristic by Dorigo et al. [6]. The observation of foraging behavior of ant species inspired the ACO technique development as a stochastic local search method. For instance, ants locate the shortest path between the ant colony and a food source by exchanging information about the route that should be followed. When the ants walk to and from the food source, they leave pheromones on the ground; this pheromone trail is used by ants to communicate with each other. Ants probabilistically prefer to follow a direction proportional to the quantity of pheromone [6]. Using simple reactive agents allows the transition from the natural to artificial ant colony. These agents cooperate by exchanging information through environment modifications. That is, artificial ants communicate indirectly via artificial pheromone trails.

The proposed approach uses a specific number of ants moving on the image driven by the local image intensity values variation. This variation establishes a pheromone matrix, with the same size image, which represents the edge information at each image pixel location [27]. Due to the large image size and to reduce computation time, the ACO algorithm described below was independently applied on non-overlapping 128 × 128 image windows.

ACO is an iterative algorithm. At each iteration, a number of artificial ants are considered. Each builds a solution over the solution space through their movements and by updating pheromone information. The process starts with an initialization stage, and then runs for N iterations to construct the pheromone matrix by iteratively performing construction and update processes.

Suppose that K ants are used to find the optimal solution (image edges) in a space χ; that is, in a sub-image I with size $M_1 \times M_2$, and where each pixel can be viewed as a node, the ACO algorithm implemented could be summarized as follows:

1. *Determine the heuristic information and initialize the resultant image* $I_{res} = 0$
2. *For each original* 128×128 *image window*
   a. *Randomly initialize the positions of the K ants and the pheromone matrix* $\tau^{(0)}$.
   b. *For the construction step index n = 1:N*
      i. *For the ant index k = 1:K*
         1. *Consecutively move the* k^{th} *ant for L steps, according to the probabilistic transition matrix* $p^{(n)}$ *(with a size of* $M_1M_2 \times M_1M_2$*).*
         2. *Local update of the pheromone matrix*
      ii. *End For*
      iii. *Global update of the pheromone matrix*
   c. *End For*
3. *Assign pheromone matrix* $\tau^{(N)}$ *to the correspondent window on the resultant image*
4. *End For*

This algorithm contains two crucial issues that have to be considered in the ACO process: the establishment of the probabilistic transition matrix $p^{(n)}$ and the pheromone matrix update. For the former, a probabilistic action rule determined by Dorigo et al. [6] was used:

$$p^{n}_{(l,m),(i,j)} = \frac{\left(\tau^{(n-1)}_{i,j}\right)^{\alpha}(\eta_{i,j})^{\beta}}{\sum_{(i,j)\in\Omega_{(l,m)}}\left(\tau^{(n-1)}_{i,j}\right)^{\alpha}(\eta_{i,j})^{\beta}}, \quad \text{if } (i,j) \in \Omega_{(l,m)} \tag{1}$$

Eq. (1) indicates the probability that at the n-th construction step of ACO, the k-th ant moves from node (l, m) to node (i, j). is the pheromone information value of the arc linking the two nodes under consideration; $\Omega_{(l,m)}$ is the set of feasible components, that is, edges $((l, m), (i, j))$ where (i, j) is a node not yet visited by ant k; α and β are constants that represent the influence of pheromone and heuristic information, respectively; $\eta_{i,j}$ represents the heuristic information for going from node (l, m) to node (i, j), fixed to be the same for each construction step. In [27], this parameter was determined by local statistics at the pixel position (i, j) as

$$\eta_{i,j} = \frac{1}{Z}V_c(I_{i,j}) \tag{2}$$

where $Z = \sum_{i=1:M_1}\sum_{j=1:M_2}V_c(I_{i,j})$ is a normalization factor, $I_{i,j}$ is the pixel intensity value at position (i, j) of image I, and the function $V_c(I_{i,j})$ is a function of a local group of pixels. The value of this function depends on the image's intensity values variation on this group of pixels with the shape shown in Fig. 4. Consequently, for pixel $I_{i,j}$, the function $V_c(I_{i,j})$ is

$$\begin{aligned} V_c(I_{i,j}) = f(&|I_{i-2,j-1} - I_{i+2,j+1}| + |I_{i-2,j+1} - I_{i+2,j-1}| + |I_{i-1,j-2} - I_{i+1,j+2}| + |I_{i-1,j-1} - I_{i+1,j+1}| + |I_{i-1,j} - I_{i+1,j}| + |I_{i-1,j+1} \\ &- I_{i+1,j-1}| + |I_{i-1,j+2} - I_{i+1,j-2}| + |I_{i,j-1} - I_{i,j+1}|) \end{aligned} \tag{3}$$

In order to establish function $f(\cdot)$ in Eq. (3), the function mathematically expressed in Eq. (4) was used. The parameter λ adjusts the function's shape. The quadratic function was chosen because it enhances the highest gray levels, representing an advantage in this case as appropriate for exudates.

$$f(x) = \lambda x^2, \quad \text{for } x \geqslant 0 \tag{4}$$

As far as the pheromone matrix is considered, two updates are needed during the ACO process. The first update occurs after the movement of each ant within each construction step. This update is performed using the following equation

$$\tau^{(n-1)}_{i,j} = \begin{cases} (1-\rho)\cdot\tau^{(n-1)}_{i,j} + \rho\cdot\Delta^{(k)}_{i,j}, & \text{if } (i,j) \text{ is visited by the current k-th ant} \\ \tau^{(n-1)}_{i,j}, & \text{otherwise} \end{cases} \tag{5}$$

where ρ is the evaporation rate, $\Delta^{(k)}_{i,j}$ in this particular case is determined by the heuristic matrix, that is, $\Delta^{(k)}_{i,j} = \eta_{i,j}$. The second update occurs after the movement of all K ants within each construction step, and the matrix is updated according to

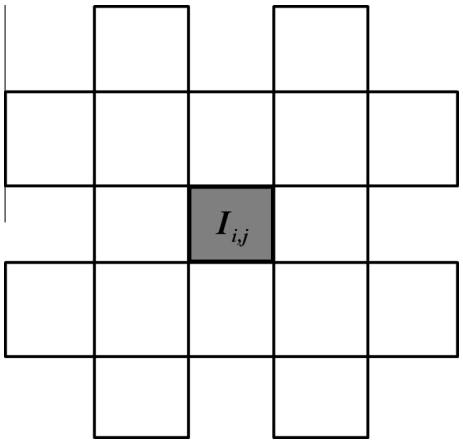

Fig. 4. Local configuration at the pixel $I_{i,j}$ for determining the variation V_c.

$$\tau^{(n)} = (1 - \varphi) \cdot \tau^{(n-1)} + \varphi \cdot \tau^{(0)} \tag{6}$$

where $\varphi \in (0, 1]$ is the pheromone decay coefficient.

The ACO algorithm parameters are described in Table 2. Another issue that has to be established is the permissible range of the ant movement ($\Omega_{(l,m)}$) In this paper, the 8-connectivity proposed in paper [27] was chosen.

2.3. Exudate detection

From the I_{cand} image, the object candidates were obtained using 8-neighbor connected component analysis. As proposed by Sanchez et al. [24], the edge strength of each object candidate was determined as the mean intensity under the object in the edge-enhanced image resultant from the ACO algorithm step. A candidate was then considered an exudate if its edge strength value is bigger than a threshold (th). th is an algorithm parameter that determines the minimum value that an edge must have to be considered a sharp boundary. To detect more exudates, a low value has to be chosen, but false positives also increase.

To reduce the number of false positives that usually appear close to blood vessels, the segmented vasculature map obtained with Zana and Klein's method [30] was used to eliminate the blood vessels' edges found by the ACO algorithm. Then, to evaluate the final output, the following thresholds were used: $th \in \{0{:}0.005{:}0.2\}$.

2.4. Giancardo et al.'s approach [9]

Giancardo et al.'s approach is, similar to the proposed method, constituted by two main parts. First, the intensity component of the Hue, Saturation, and Intensity (HIS) color space was used to estimate the background image. Then, a morphological reconstruction step was applied to enhance the normalization as it seemed to improve the removal of the nerve fiber layer and other structures close to the OD. After normalization, a small hard threshold was applied, and candidates were selected from the resultant image. For each exudate candidate, edge strength was defined by the average intensity under the candidate in the Kirsch resultant image. The Kirsch filter was applied in the original image green plane. Fig. 5 illustrates the schematic of this method.

Table 2
ACO algorithm parameters values.

Parameter	Value
K – total number of ants	$\lfloor\sqrt{M_1 \times M_2}\rfloor$
τ_{init} – initial value of each component of the pheromone matrix	0.0001
α – weighting factor of the pheromone information	1
β – weighting factor of the heuristic information	0.1
λ – adjusting factor of the functions in (8)–(11)	10
ρ – evaporation rate	0.1
L – total number of ant's movement steps within each construction step	300
ψ – pheromone decay coefficient	0.05
N – total number of construction steps	3

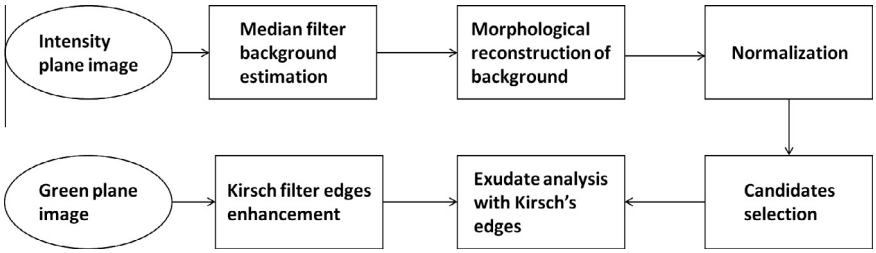

Fig. 5. Schematic representation of Giancardo et al.'s approach with the Kirsch filter.

To make a fair comparison between Giancardo et al.'s approach and ours, we added a step to the former. The segmented vasculature map used in the present approach was added to eliminate the blood vessels' edges enhanced by the Kirsch filter.

Giancardo et al.'s study also used stationary wavelets to evaluate the peak intensity of each candidate [9]. However, they reported [9] that the Kirsch approach generally showed better results. Moreover, our method follows the same idea of the Giancardo et al. Kirsch approach since the candidates are evaluated in terms of edge strength. In that way, in this study we compared our system with the Giancardo et al. approach that used Kirsch edges.

2.5. Fundus images and system performance evaluation

The HEI-MED (Hamilton Eye Institute Macular Edema Dataset), a publicly available dataset developed by Giancardo et al. [10], was used to test the approaches. This dataset is composed of 169 images representative of various degrees of DR. The images present great variability since they belong to patients of different ages and ethnicities. Moreover, the dataset contains the bright lesion manual segmentation for each image, where the exudates are distinguished from other bright lesions, such as cotton wool spots and drusen.

To evaluate the performance of the approaches, two criteria were used: the pixel-based criterion and the image-based criterion. For the first, all pixels belonging to a candidate that partially or totally overlaps a manually segmented bright lesion were considered True Positive (TP). All candidate pixels outside this criterion were registered as False Positives (FP). All exudate pixels manually segmented that were not segmented by this approach were considered False Negatives (FN). In the image-based criterion, the capacity of the algorithm to exclude healthy images was evaluated. An image was considered healthy if it did not contain any exudate and pathological if it contained at least one exudate.

Researchers frequently evaluate their approaches' performance in terms of sensitivity (Eq. (7)) versus predictive positive value (Eq. (8)) (see Table 1). However, this does not seem to be a good quantitative evaluation since the predictive positive value depends on prevalence. Therefore, if images have a large quantity of exudates, the prevalence would naturally be bigger than in images with few exudates. To avoid this, in the present approach we also evaluated the receiver operating characteristic (ROC) curves, which plot the true positive rate (Sensitivity) in function of the false positive rate (1-Specificity). Therefore, to determine the ROC curve, specificity values must be calculated (Eq. (9)). The problem in calculating the specificity is that if all image pixels are considered, the number of true negative (TN) pixels will be huge compared with the FP values, and thus, specificity will always have high values. To overcome this problem, we propose to calculate the TN as a function of the threshold value (Eq. (10)). When *th* is 0, the FP number has its maximum. Increasing *th* by 0.005, the FP number decreases, and pixels that were false positive became true negative pixels (Fig. 6). On the other side, the TN number has its minimum when $th = 0$, and afterward, it increases with the threshold variation. In that way, if the TN number is considered zero when $th = 0$, then its value can be compared with the FP number, and the specificity value will be more representative of the approach capacity to exclude pixels that are not exudates. In this study, ROC curves were constructed following this idea.

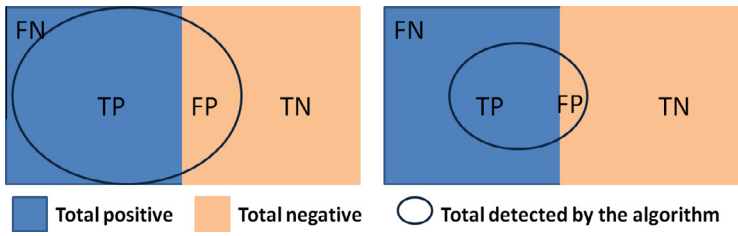

Fig. 6. Schematic representing statistical measures: FN, TP, TN and FP. From left to right represents what happens when threshold increases: the TP and FP decreases and becomes FN and TN, respectively.

In addition to the ROC curves, the approaches were also evaluated in terms of accuracy (Eq. (11)).

$$Sensitivity = \frac{TP}{TP + FN} \tag{7}$$

$$PPV = \frac{TP}{TP + FP} \tag{8}$$

$$Specificity = \frac{TN}{TN + FP} \tag{9}$$

$$TN(th) = FP(th - 0.005) - FP(th) + TN(th - 0.005) \tag{10}$$

$$Accuracy = \frac{TP + TN}{TP + FP + FN + TN} \tag{11}$$

3. Results and discussion

The results of the proposed approach applied to images with exudates from the HEI-MED dataset are shown in Fig. 7. It illustrates (from left to right): original color image, the binary image resulting from the preprocessing step with the exudate candidates, gray-level image resulting from the ACO algorithm; and the green plane image with the exudates segmented by the proposed approach. From the preprocessing phase, a binary image with all exudates segmented, and many false positives resulted. The ACO algorithm image reveals enhancement of the exudate edges. The combination of both images taking into account the edge strength of each candidate can remove most of the FP pixels.

The lesion segmentation performance of the proposed algorithm was evaluated by determining the overall sensitivity, specificity, accuracy, and predictive positive values for each threshold value. Fig. 8 illustrates the proposed approach and the Kirsch approach ROC curves and the respective area under the curve (AUC) values. AUC is an accuracy measure; that is, it measures the approach capacity to distinguish between normal and exudate pixels. Therefore, the proposed approach performs better than the Kirsch approach since the respective AUC values are 0.975 against 0.971. Since the candidates of both approaches were obtained with different processes, Fig. 8 also contains the ROC curve of a different approach that begins with our candidate detection method and uses the Kirsch filter to enhance the edges. The respective AUC demonstrates that the ACO edge enhancement method performs better than the Kirsch filter.

Table 3 shows the quantitative results for these three approaches when the overall accuracy reaches its maximum. The three methods can be compared. The new approach performs somewhat better in terms of sensitivity.

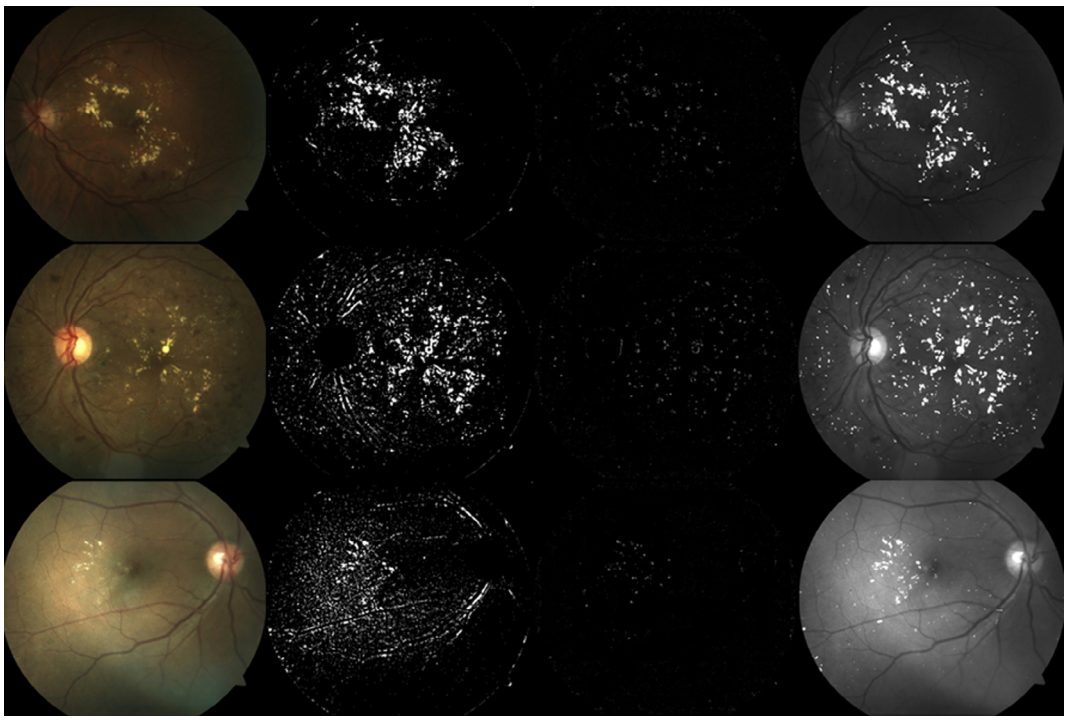

Fig. 7. From left to right: original color image; binary image with exudate candidates (I_{cand}); ACO algorithm gray-level image; green plane image with the exudate segmentation. (For interpretation of the references to color in this figure legend, the reader is referred to the web version of this article.)

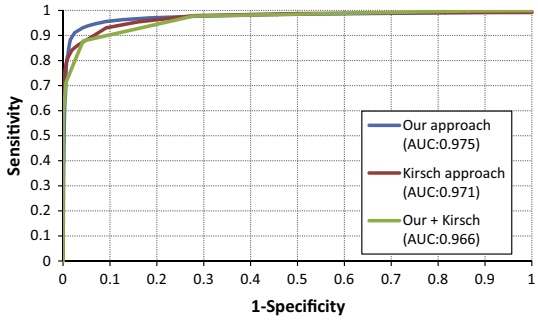

Fig. 8. ROC curves using all images and the pixel-based criterion.

Although the performance evaluation is important in terms of the pixel-based criterion, the image-based criterion is crucial when goal is the development of a system for diagnosing diabetic retinopathy. Thus, detecting a single exudate in an image with many of them is as useful and important as detecting an exudate in an image with only one lesion of this type. Consequently, the algorithm's capacity to distinguish patients with or without bright lesions should be evaluated. Fig. 9 illustrates the ROC curves of the proposed and Kirsch approaches calculated with all images from the HEI-MED dataset and using the image-based criterion. Although the AUC value for the Kirsch method is higher than that for the proposed approach, the discrepancy is very small. Furthermore, the shape of the curves is irregular and intersects several times, indicating that for some threshold values, the proposed approach has a better performance than the Kirsch approach. For other threshold values, the opposite is observed. The point is that none of the approaches perform as needed for clinical practices and both need improvements. The same applies to the approaches found in the literature described in Section 1. A comparison between our approach and those found in the literature is not always possible, since the retinal images dataset and the quantitative metrics used were not the same. Therefore, we limited our comparison with the segmentation step of the Giancardo et al. approach [10] that was described in a previous work [9], since we used their database.

The contributions of this study include the use of a dataset available online, which permits future comparisons with other approaches, and the development of a new unsupervised method for detecting exudates. In addition, the application of an ant colony to locally explore the image gray-level variation is the greatest novelty of this study. Using global approaches such as traditional algorithms leads to rigid systems that cannot be adapted and generalized to unknown situations. This is the reason in the last few years researchers have been working in multi-agent systems (MASs) applied to digital image processing [18]. In fact, each agent can locally process image information and deliberate according to the agent's perceptions from the environment and agents surrounding it. The ACO algorithm can be called an agent-based algorithm since this algorithm is constituted by a number of agents with memory moving on the image (environment) and that communicates indirectly through the environment [5]. Moreover, through self-organizing dynamics driven by local interactions and communications

Table 3
Quantitative results using the pixel-based criterion for the three approaches and using all images.

Approach	Accuracy	Sensitivity	Specificity	PPV
Our	0.9785	0.8082	0.9916	0.7301
Kirsch	0.9767	0.7575	0.9961	0.8348
Our + Kirsch	0.9786	0.5986	0.9988	0.8944

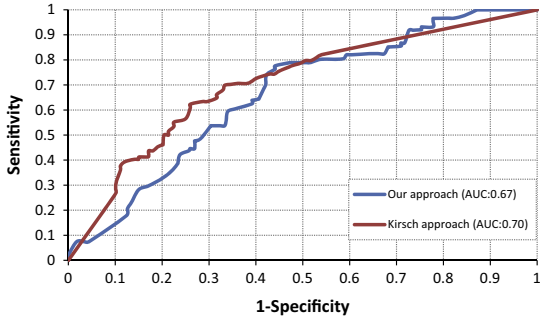

Fig. 9. ROC curves using all images and the image-based criterion.

between ant-like agents, a complex global behavior emerges, which, in this case, consists of enhancing the edges. However, not all the possibilities of MASs were used in the proposed approach. As future work, the development of a more complex agent society that uses all the advantages of MASs could increase the algorithm capacity to generalize and improve its performance. Furthermore, with the same system it can be possible to segment other diabetic retinopathy characteristic lesions and classify the DR stage.

4. Conclusion

In this paper, a new algorithm based on ACO is described for detecting exudates in color fundus images. The ACO algorithm was used as an edge detector and revealed good capacity to generalize since the algorithm enhances edges well in images with great variability inside and between them.

The performance of the proposed approach was evaluated using a dataset available online, which allows future comparisons with other systems. Comparing this approach with state-of-the-art methods is not always possible because most use private datasets and different quantitative metrics. Therefore, we decided to confine our evaluation with a very recent state-of-the-art method. Using the pixel-based criterion, the experimental results show that the proposed approach yields a better AUC than Giancardo et al.'s method with Kirsch filter.

The use of an ant colony is the main contribution of this study as this is a novelty and presents MAS characteristics. Therefore, as future work, exploring all the possibilities of MASs for improving the system could be an effective method for diagnosing DR through fundus image analysis.

A new category of approaches based on MASs is being applied to retinal images. With MASs, we are trying to overcome the drawbacks of traditional algorithms by including cooperation between methods and adaptation to the local situations in the image.

References

[1] M. Akram, A. Tariq, S.A. Khan, M.Y. Javed, Automated detection of exudates and macular of grading of diabetic macular edema, Comput. Methods Prog. Biomed. 114 (2014) 141–152.
[2] S. Ali, D. Sidibé, K.M. Adal, L. Giancardo, E. Chaum, T.P. Karnowski, F. Mériaudeau, Statistical atlas based exudate segmentation, Comput. Med. Imag. Graph. 37 (2013) 358–368.
[3] F. Amel, M. Mohammed, B. Abdelha_d, Improvement of the hard exudates detection method used for computer-aided diagnosis of diabetic retinopathy, Int. J. Image, Graph. Signal Process. (IJIGSP) 4 (4) (2012) 19–27.
[4] M. Cinsdikici, D. AydIn, Detection of blood vessels in ophthalmoscope images using MF/ant (matched filter/ant colony) algorithm, Comput. Methods Prog. Biomed. 96 (2) (2009) 85–95.
[5] G. Di Caro, Ant colony optimization and its application to adaptive routing in telecommunication networks, Fac. Sci. Appl. (2004).
[6] M. Dorigo, M. Birattari, T. Stutzle, Ant colony optimization, Comput. Intell. Mag., IEEE 1 (4) (2006) 28–39.
[7] A. Fleming, S. Philip, K. Goatman, G. Williams, J. Olson, P. Sharp, Automated detection of exudates for diabetic retinopathy screening, Phys. Med. Biol. 52 (2007) 7385–7396.
[8] M. García, C. Sánchez, M. López, D. Abásolo, R. Hornero, Neural network based detection of hard exudates in retinal images, Comput. Methods Prog. Biomed. 93 (1) (2009) 9–19.
[9] L. Giancardo, F. Meriaudeau, T. Karnowski, Y. Li, K. Tobin, E. Chaum, Automatic retina exudates segmentation without a manually labelled training set, in: 2011 IEEE International Symposium on Biomedical Imaging: From Nano to Macro, IEEE, 2011, pp. 1396–1400.
[10] L. Giancardo, F. Meriaudeau, T. Karnowski, Y. Li, S. Garg, K. Tobin, E. Chaum, Exudate-based diabetic macular edema detection in fundus images using publicly available datasets, Med. Image Anal. 16 (2012) 216–226.
[11] S. Hooshyar, R. Khayati, Retina vessel detection using fuzzy ant colony algorithm, in: 2010 Canadian Conference on Computer and Robot Vision (CRV), IEEE, 2010, pp. 239–244.
[12] R. Hornero, M. Aboy, J. Poza, et al, A novel automatic image processing algorithm for detection of hard exudates based on retinal image analysis, Med. Eng. Phys. 30 (3) (2008) 350–357.
[13] P. Huang, H. Cao, S. Luo, An artificial ant colonies approach to medical image segmentation, Comput. Methods Prog. Biomed. 92 (3) (2008) 267–273.
[14] G. Kavitha, S. Ramakrishnan, An approach to identify optic disc in human retinal images using ant colony optimization method, J. Med. Syst. 34 (5) (2010) 809–813.
[15] H. Li, O. Chutatape, Automated feature extraction in color retinal images by a model based approach, IEEE Trans. Biomed. Eng. 51 (2) (2004) 246–254.
[16] L. Ma, J. Tian, W. Yu, Visual saliency detection in image using ant colony optimization and local phase coherence, Electron. Lett. 46 (15) (2010) 1066–1068.
[17] L. Ma, K. Wang, D. Zhang, A universal texture segmentation and representation scheme based on ant colony optimization for iris image processing, Comput. Math. Appl. 57 (11–12) (2009) 1862–1868.
[18] J. Mahdjoub, Vers un système de vision auto-adaptatif à base de systems multi-agents, Centre de Recherche en STIC (CReSTIC/SIC), 2011.
[19] A. Malisia, H. Tizhoosh, Image thresholding using ant colony optimization, in: The 3rd Canadian Conference on Computer and Robot Vision, 2006, IEEE, 2006.
[20] M. Niemeijer, B. van Ginneken, S. Russell, M. Suttorp-Schulten, M. Abràmoff, Automated detection and differentiation of drusen, exudates, and cotton-wool spots in digital color fundus photographs for diabetic retinopathy diagnosis, Invest. Ophthalmol. Vis. Sci. 48 (5) (2007) 2260–2267.
[21] A. Osareh, B. Shadgar, R. Markham, A computational-intelligence-based approach for detection of exudates in diabetic retinopathy images, IEEE Trans. Inform. Technol. Biomed. 13 (4) (2009) 535–545.
[22] C. Pereira, L. Gonçalves, M. Ferreira, Optic disc detection in color fundus images using ant colony optimization, Med. Biol. Eng. Comput. 51 (3) (2012) 295–303.
[23] S. Ravishankar, A. Jain, A. Mittal, Automated feature extraction for early detection of diabetic retinopathy in fundus images, in: IEEE Conference on Computer Vision and Pattern Recognition, 2009, CVPR 2009, IEEE, 2009, pp. 210–217.
[24] C. Sánchez, M. García, A. Mayo, M. López, R. Hornero, Retinal image analysis based on mixture models to detect hard exudates, Med. Image Anal. 13 (4) (2009) 650–658.
[25] A. Sopharak, B. Uyyanonvara, S. Barman, T. Williamson, Automatic detection of diabetic retinopathy exudates from non-dilated retinal images using mathematical morphology methods, Comput. Med. Imag. Graph. 32 (8) (2008) 720–727.
[26] W. Tao, H. Jin, L. Liu, Object segmentation using ant colony optimization algorithm and fuzzy entropy, Pattern Recogn. Lett. 28 (7) (2007) 788–796.

[27] J. Tian, W. Yu, S. Xie, An ant colony optimization algorithm for image edge detection, in: IEEE Congress on Evolutionary Computation, 2008, CEC 2008 (IEEE World Congress on Computational Intelligence), IEE, 2008, pp. 751–756.
[28] T. Walter, J. Klein, P. Massin, A. Erginay, A contribution of image processing to the diagnosis of diabetic retinopathy-detection of exudates in color fundus images of the human retina, IEEE Trans. Med. Imag. 21 (10) (2002) 1236–1243.
[29] D. Welfer, J. Scharcanski, D. Marinho, A coarse-to-fine strategy for automatically detecting exudates in color eye fundus images, Comput. Med. Imag. Graph. 34 (3) (2010) 228–235.
[30] F. Zana, J. Klein, Segmentation of vessel-like patterns using mathematical morphology and curvature evaluation, IEEE Trans. Image Process. 10 (7) (2001) 1010–1019.
[31] J. Zhang, K. He, J. Zhou, M. Gong, Ant colony optimization and statistical estimation approach to image edge detection, in: 2010 6th International Conference on Wireless Communications Networking and Mobile Computing (WiCOM), IEEE, 2010, pp. 1–4.
[32] X. Zhang, Exudate detection in color retinal images for mass screening of diabetic retinopathy, Med. Image Anal. 18 (7) (2014) 1026–1043.